

# Electron energy loss spectroscopy of plasmon resonances in titanium nitride thin films

Cite as: Appl. Phys. Lett. **108**, 171107 (2016); <https://doi.org/10.1063/1.4947442>

Submitted: 11 February 2016 • Accepted: 12 April 2016 • Published Online: 29 April 2016

Andrew A. Herzing,  Urcan Guler,  Xiuli Zhou, et al.



View Online



Export Citation



CrossMark

## ARTICLES YOU MAY BE INTERESTED IN

[Temperature-dependent optical properties of titanium nitride](#)

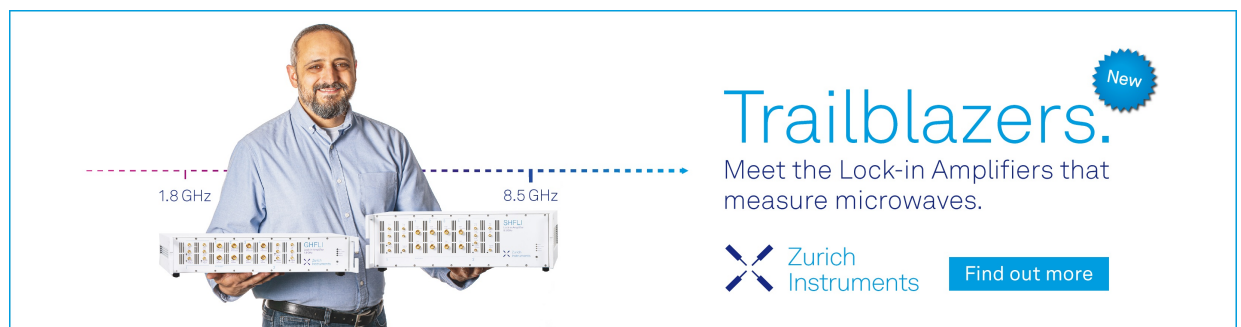
Applied Physics Letters **110**, 101901 (2017); <https://doi.org/10.1063/1.4977840>


[Electronic and optical properties of titanium nitride bulk and surfaces from first principles calculations](#)

Journal of Applied Physics **118**, 195302 (2015); <https://doi.org/10.1063/1.4935813>


[Optical, electronic, and transport properties of nanocrystalline titanium nitride thin films](#)

Journal of Applied Physics **90**, 4725 (2001); <https://doi.org/10.1063/1.1403677>



**Trailblazers.** 

Meet the Lock-in Amplifiers that measure microwaves.

 Zurich Instruments [Find out more](#)



## Electron energy loss spectroscopy of plasmon resonances in titanium nitride thin films

Andrew A. Herzing,<sup>1,a)</sup> Urcan Guler,<sup>2,3</sup> Xiuli Zhou,<sup>4</sup> Alexandra Boltasseva,<sup>2</sup> Vladimir Shalaev,<sup>2</sup> and Theodore B. Norris<sup>4</sup>

<sup>1</sup>Material Measurement Laboratory, National Institute of Standards and Technology, Gaithersburg, Maryland 20899, USA

<sup>2</sup>School of Electrical and Computer Engineering and Birck Nanotechnology Center, Purdue University, West Lafayette, Indiana 47907, USA

<sup>3</sup>Nano-Meta Technologies, Inc., 1281 Win Henschel Boulevard, West Lafayette, Indiana 47906, USA

<sup>4</sup>Center for Ultrafast Optical Science, University of Michigan, Ann Arbor, Michigan 48109, USA

(Received 11 February 2016; accepted 12 April 2016; published online 29 April 2016)

The plasmon resonance characteristics of refractory TiN thin films were analyzed using electron energy-loss spectroscopy (EELS). A bulk plasmon resonance was observed at 2.81 eV and a weaker surface plasmon resonance peak was detected at 2.05 eV. These findings are compared to finite-difference time-domain simulations based on measured optical data. The calculated values for both the bulk and surface resonances (2.74 eV and 2.15 eV, respectively) show reasonable agreement with those measured via EELS. The amplitude of the experimentally observed surface resonance was weaker than that typically encountered in noble metal nanostructures, and this is discussed in the context of electron density and reduced spatial confinement of the resonance mode in the thin-film geometry. *Published by AIP Publishing.* [<http://dx.doi.org/10.1063/1.4947442>]

The interaction of light with free electrons in metallic nanostructures via excitation of plasmonic resonances offers a promising route to controlling the properties and propagation of light at the length scales far below the optical diffraction limit.<sup>1</sup> These plasmonic nanostructures typically consist of noble metals, and can exhibit very strong, well-defined resonances in the ultra-violet, visible, and near-infrared regions of the electromagnetic spectrum.<sup>2</sup> However, the promise of this technology has yet to be fully realized due to inherent limitations in the constituent materials, which often result in heavy losses in the optical frequency range.<sup>3</sup> Additionally, noble metals suffer from poor chemical and/or thermal stability, and are often incompatible with microelectronic processing technology, thus severely restricting their use in practical applications.

Recently, refractory transition metal nitrides have been proposed as an alternative class of materials for practical plasmonic applications.<sup>4</sup> In particular, TiN has been found to display a number of promising properties.<sup>5,6</sup> Exhibiting optical properties similar to those of gold, TiN is promising for several applications and stands out with its superior material properties. As a refractory material, TiN is durable at extremely high temperatures and resistant to chemically aggressive environments.<sup>7</sup> Furthermore, TiN is fully compatible with the existing CMOS fabrication techniques and biocompatibility of the material makes it favorable for applications with process-related restrictions.<sup>8–10</sup>

Characterization of the plasmonic response of a material is usually carried out via optical techniques. However, spatial resolution is limited by diffraction in far-field methods and limited by the tip dimensions in near-field techniques; near-field optical scanning microscopy cannot generally achieve the single-nm resolution required to map plasmon modes in detail or to measure local variations due to changes in structure or chemistry on the required length scale.<sup>11</sup> This

limitation is particularly troublesome for transition metal nitrides such as TiN, since local variations in chemistry could have an unknown effect on the optical behavior. TiN can be found in a wide range of compositions due to the presence of vacancies on the nitrogen sublattice of the NaCl-type structure, and oxidation is known to occur in a limited fashion upon exposure to air.

In contrast to optical methods, electron energy-loss spectroscopy (EELS) in a monochromated scanning transmission electron microscope (STEM) offers a method for assessing the dielectric properties of materials using a sub-nanometer sized probe with an energy-resolution below 0.2 eV.<sup>12–16</sup> In fact, many of the early observations of surface plasmons were reported using EELS for the study of thin metal films.<sup>17</sup> EELS can also provide a measure of the local composition and is readily combined with atomic-resolution real-space imaging for structural evaluation. In this paper, we characterized the local plasmonic response in TiN thin films via high-resolution EELS using both experimental and theoretical/numerical approaches. These results will form the basis for further study of more complex plasmonic nanostructures consisting of advanced plasmonic materials.

Thin films of TiN were deposited onto an MgO substrate via DC magnetron sputtering of a titanium target in a mixed gaseous environment of argon and nitrogen flowing at 4 sccm and 6 sccm, respectively. The chamber base pressure was  $1.1 \times 10^{-5}$  Pa ( $8.0 \times 10^{-8}$  Torr) and the substrate temperature was 800 °C during deposition. TiN films were deposited with a target thickness of 100 nm using a growth rate of 1.5 nm/min. Optical characterization was subsequently performed over a wavelength range of 300 nm–2000 nm via variable angle spectroscopic ellipsometry with incidence angles of 65°, 70°, and 75°.

Cross-sectional specimens of the TiN film were prepared for STEM analysis using a focused ion-beam (FIB) system (FEI Nova Nanolab 600) using a standard lift-out

<sup>a)</sup>Electronic mail: andrew.herzing@nist.gov

procedure.<sup>18</sup> Briefly, a rectangular region of the film is protected using sequential deposition of electron-beam and ion-beam assisted deposition of carbon. Next, ion-assisted deposition of  $\approx 1.5 \mu\text{m}$  of Pt is carried out to further protect the specimen during preparation. This is followed by selective removal of the surrounding material on either side via milling with a 30 keV focused Ga beam. The exposed section was then lifted free from the bulk using a micromanipulator, micro-welded to a STEM-compatible Cu support, and thinned to electron transparency using the 30 keV Ga beam. Finally, the specimen surface was polished using a 5 keV Ga beam in an effort to remove re-deposited material and any amorphous surface layer produced by the more intensive ion milling procedure.

The resulting lamellae were then analyzed using STEM high-angle annular dark-field (HAADF) imaging and EELS using an FEI Titan 80–300 TEM/STEM using a monochromated 150 keV electron beam. The instrument was equipped with a Gatan Tridiem 865 imaging energy filter producing a final spectral resolution of less than 0.2 eV as measured by the full-width at half maximum of the EELS zero-loss peak (ZLP). The through-specimen thickness (i.e., in the direction of the incident beam) was determined to be  $\approx 135 \text{ nm}$  by analysis of a low-loss EELS spectra collected from the MgO substrate. Spatially resolved EELS measurements of the low-loss response were performed using a probe current of 20 pA, and data processing was carried out using the Gatan Digital Micrograph software suite. In order to interpret the inelastic scattering profile properly, the tails from the zero-loss peak (ZLP) were removed by fitting a power-law decay function to a region of the spectrum just prior to the onset of inelastic scattering.<sup>19</sup> This function was then extrapolated towards higher energy-loss subtracted from the input spectrum. In order to determine the elemental composition in the film, core-loss EELS spectra were collected in a similar fashion using a probe current of 200 pA. Quantification was performed in the Gatan Digital Micrograph software suite using the N K-edge and the Ti  $L_{2,3}$ -edge.

The results have been interpreted via numerical solution of the Maxwell equations using the finite-difference time-domain (FDTD) Lumerical package, calculating the response arising from excitation by an optical dipole source at different positions relative to the TiN film. This approach mimics the incident electron beam by calculating the optical transmission spectra, and has been demonstrated to agree with results produced from direct calculation of the energy loss.<sup>20,21</sup> The frequency dependent dielectric function of TiN used in the simulations was obtained via optical ellipsometry measurements across the visible and near-infrared spectrum of equivalent TiN samples grown under the same conditions, and these are shown in supplementary Figure S2.<sup>22</sup> Dielectric constants for the MgO substrate and Pt support layer were obtained from the SOPRA optical database.

STEM-HAADF analysis of the cross-sectional FIB specimen showed the film to be  $\approx 93 \text{ nm}$  as measured from the onset of scattering from the MgO substrate to that of the protective layer deposited via FIB. High magnification imaging of the MgO-TiN interface (Fig. 1) revealed a high degree of continuity of the lattice planes across the interface, which demonstrates that the growth of the TiN film proceeds epitaxially due

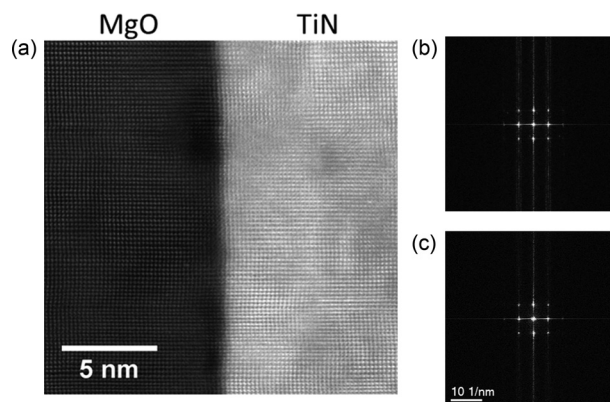


FIG. 1. STEM-HAADF image (a) of the interface between the MgO substrate and TiN showing epitaxial growth and high degree of crystal quality in the as-grown film. Also shown are the fast Fourier-transforms (FFTs) extracted from the MgO (b) and TiN (c) portions of the image. The lattice spacing in the growth direction was measured to be 0.212 nm in both the substrate and film.

to the similarity in the two crystal structures. Fast Fourier transforms (FFT's) extracted from the MgO substrate and TiN film regions are also shown (Figs. 1(b) and 1(c)). In both cases, the measured lattice spacing in the growth direction was 0.21 nm, which agrees well with that expected for the (200) planes in the bulk crystals (ICSD entries 01–071–1176 and 00–038–1420, respectively). No extended defects were detected at any point along the analyzed width of the film ( $\approx 1 \mu\text{m}$ ).

Finally, the elemental composition and homogeneity of the film were inspected using core-loss EELS of the Ti- $L_{2,3}$  and N-K edges (located at 455.5 eV and 401.6 eV, respectively). No significant variation in stoichiometry was detected between the region near the MgO interface and the interior of the film. The film composition at these locations was found to be  $(55.1 \pm 1.5)\%$  Ti (atom fraction) as independently calculated from over 500 individual spectra. In addition, no oxygen was detected at any position within the TiN film. It should be noted that detection of trace amounts of oxygen in this case is complicated due to the position of the oxygen K-edge relative to the titanium L-edge in the EELS spectrum, where the former is positioned at approximately 75 eV greater energy loss than the latter. Because of this, the post-edge intensity of the Ti signal extends beyond the onset energy of the oxygen edge and therefore contributes non-trivially to the background intensity beneath the edge. This slightly increases the minimum detectable mass of oxygen from the more idealized case where titanium is not present and the pre-edge background signal is less intense. Therefore, the presence of a small amount of oxygen in the specimen cannot be ruled out.

Valence loss EELS results are presented in Figure 2. Starting in the MgO substrate, spectra were collected in 0.5 nm increments along a 150 nm line (yellow arrow in Figure 2(a)) across the entire width of the TiN film and terminating in the FIB-deposited protective over-layer. Spectra extracted from the MgO substrate, the MgO-TiN interface, and the TiN film itself are shown in Figure 2(b). In order to improve signal intensity, each plot was generated by the summation of 20 individual spectra representing a 10 nm region of the specimen along the line of acquisition. The spectrum

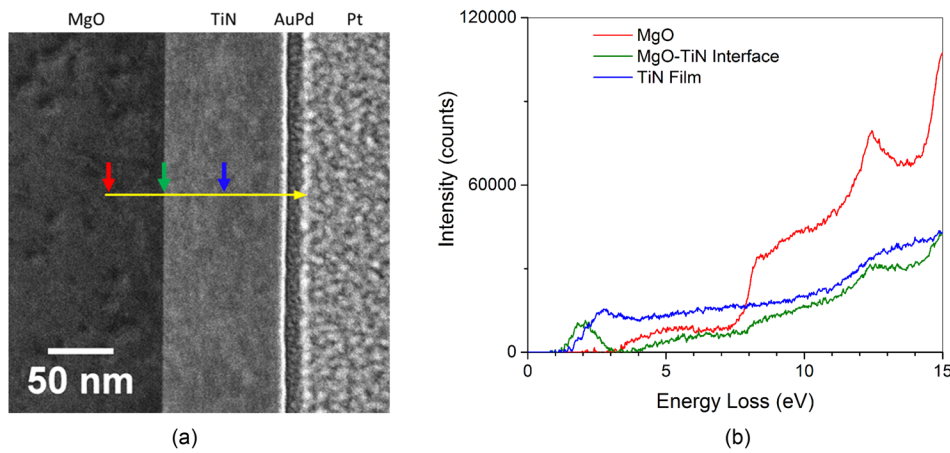


FIG. 2. STEM-HAADF image (a) showing the specimen region characterized by EELS. Spectra were collected along the yellow line beginning in the MgO substrate, traversing the TiN film, and ending in the protective Pt overlayer. Spectra integrated over ten pixels at each colored arrow are shown in (b), indicating the local inelastic scattering distribution at these locations.

from the MgO substrate exhibits spectral features typical of this material with a bandgap onset indicated by the abrupt increase in inelastic scattering near 7.5 eV.<sup>23</sup> At the junction of the MgO and TiN film, a relatively sharp peak due to surface-plasmon scattering was observed. By fitting the peak with a Gaussian function, this plasmon resonance was determined to occur at  $(2.05 \pm 0.01)$  eV. Further from the interface, at the center of the TiN film, a peak was observed at  $(2.81 \pm 0.30)$  eV. This peak was followed by a nearly linear increase in inelastic scattering probability that was continuous up until a discrete change near 11 eV.

These spectral features were measured at a variety of positions in the specimen and found to vary only slightly. Supplementary Figure S1(a) presents a series of low-loss EELS spectra as a function of distance from the MgO/TiN interface. With the exception of slight differences in intensity, no changes to the peak shape and position were observed when the beam was positioned far from the MgO/TiN interface. Some broadening of the peak width was observed in the spectrum collected closest to the interface, and this is likely due to the combined contribution of the bulk and delocalized surface plasmons at this position. This stability of the bulk plasmon position is further demonstrated in supplementary Figure S1(b), which shows the peak location of a Gaussian fit to this spectral feature over the entire thickness of the TiN film. Within the error of the fit, no difference in position was observed.

A spatially resolved map of the energy loss spectra as calculated by FDTD is presented in Figure 3(a) which shows the predicted response as a function of beam position in the region near the substrate/film interface. A magnified version of the experimental EELS data collected near the interface and from the film interior is also shown for comparison (Fig. 3(b)). For beam positions that are well within the TiN film, the calculated spectra show a primary peak at  $\approx 2.74$  eV loss; this corresponds to the bulk plasmon mode of TiN and agrees reasonably well with the experimental peak observed at 2.81 eV. When the beam is positioned within approximately 5 nm of the MgO/TiN interface, the resonance peak begins to broaden due to the development of a surface plasmon mode. This surface mode becomes more intense as the beam position approaches the interface and fully dominates in the region within (1–2) nm of the interface. The observed energy of this resonance peak continuously shifts to lower energy as

the beam approaches the interface, at which point it is observed at 2.15 eV which is only slightly higher than the peak energy observed experimentally by EELS (2.05 eV).

These results can be compared to previous reports where non-spatially resolved EELS measurements were carried out on sputtered TiN films. For example, Pflüger *et al.*<sup>24</sup> used a

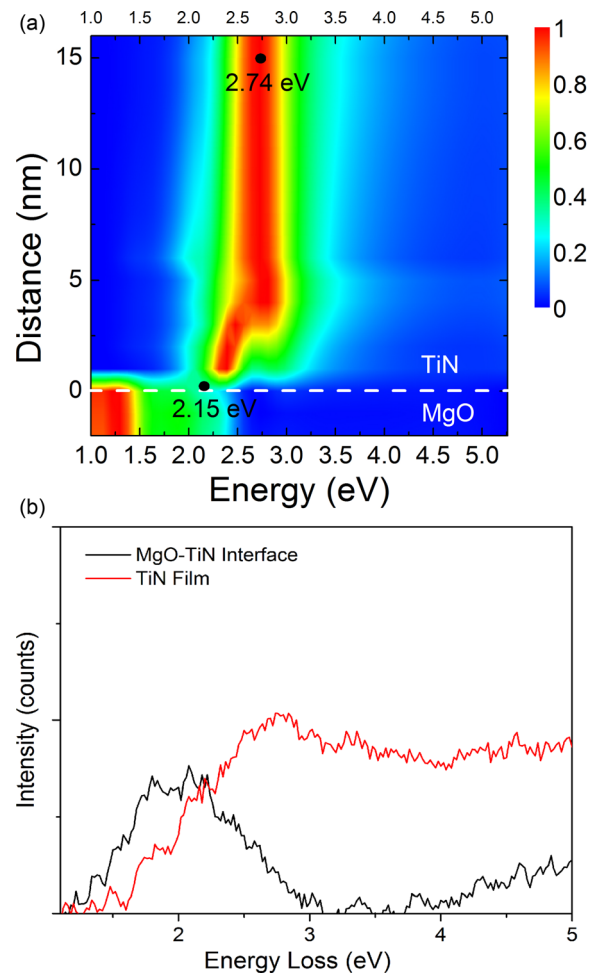


FIG. 3. Results of FDTD simulations for cross-sectional TiN thin-film on MgO substrate. Spatial map of the calculated energy-loss response as a function of position in a model MgO supported TiN film (a). Each row of the plot has been independently normalized to enable comparison between signals with varied intensity. Comparison with the experimental EELS collected at the substrate interface and the film interior (b).

monochromated 170 keV electron source to study HF-sputtered TiN films, and observed a peak at 2.8 eV loss which is quite consistent with the bulk value we have observed in STEM-EELS. In another study by Walker *et al.*,<sup>25</sup> a peak was observed at 2.3 eV in reflection EELS of a DC-magnetron sputtered films. Both studies attributed the observed peaks to Drude-like plasmon resonances, while Walker *et al.* ascribed the lower resonance value observed in their work to differences in vacancy populations between their nominally stoichiometric films and those used by Pflüger *et al.* In our case, we observe varying plasmon resonance peak energies depending upon the spatial position of the electron beam in the cross-sectional specimen, and the measured values are consistent with simulations based on measured optical data collected from the same film.

A final observation is that the amplitude of the TiN/MgO surface plasmon in the experimental EELS data is weaker than that observed from noble-metal plasmonic structures (e.g., gold and silver). This is most likely due to the presence of the insulating MgO substrate in the case of FIB-prepared sections which we have analyzed. In most cases where EELS is employed for surface plasmon resonance characterization, the beam is directed near the interface of the specimen with the surrounding ultrahigh vacuum (i.e., where  $\epsilon = 1$ ) and large peak amplitudes are observed. In the present case, the resonance develops at the interface with an insulating substrate where the dielectric environment results in a decreased plasmon scattering probability and therefore the peak amplitude is much reduced. Other factors may also play a less significant role in the lower than expected intensity of the plasmon resonance. For example, the thin-film geometry that we have studied confines the plasmon mode to a lesser degree than would other nanostructures which have been studied (rods, spheres, discs, etc.). The relative contribution of these and other factors will require additional studies over a range of specimen compositions and geometries.

In summary, we have investigated the plasmonic behavior of TiN films grown on MgO substrates. The combination of STEM-HAADF imaging with monochromated valence-loss and core-loss EELS provides a method for correlating the atomic-scale structure and chemistry with the local optical response of the material. The bulk plasmon peak position observed via EELS agrees well with an energy-loss model based on the measured optical constants. The surface plasmon resonance energy detected at the film-substrate interface also agrees well with calculations and shows a strong dependence

on the distance of the beam from the substrate/film interface. The lack of extended defects within the bulk of the film and the uniformity of composition ensure that the local response as measured by EELS can be predicted by the FDTD calculations based on high-quality optical data. Our study is foreseen to stimulate further exploration of more complex nanostructures based on these advanced plasmonic materials.

The authors acknowledge generous support from NSF MRSEC Grant No. DMR-1120923.

Any mention of commercial products is for information only; it does not imply recommendation or endorsement by NIST.

<sup>1</sup>S. A. Maier, *Plasmonics: Fundamentals and Applications* (Springer Science & Business Media, 2007).

<sup>2</sup>H. A. Atwater, *Sci. Am.* **296**, 56 (2007).

<sup>3</sup>A. Boltasseva and H. A. Atwater, *Science* **331**, 290 (2011).

<sup>4</sup>P. R. West, S. Ishii, G. V. Naik, N. K. Emani, V. M. Shalaev, and A. Boltasseva, *Laser Photonics Rev.* **4**, 795 (2010).

<sup>5</sup>U. Guler, G. V. Naik, A. Boltasseva, V. M. Shalaev, and A. V. Kildishev, *Appl. Phys. B* **107**, 285 (2012).

<sup>6</sup>G. V. Naik, J. L. Schroeder, X. Ni, A. V. Kildishev, T. D. Sands, and A. Boltasseva, *Opt. Mater. Express* **2**, 478 (2012).

<sup>7</sup>U. Guler, A. Boltasseva, and V. M. Shalaev, *Science* **344**, 263 (2014).

<sup>8</sup>U. Guler, V. M. Shalaev, and A. Boltasseva, *Mater. Today* **18**, 227 (2015).

<sup>9</sup>G. V. Naik, V. M. Shalaev, and A. Boltasseva, *Adv. Mater.* **25**, 3264 (2013).

<sup>10</sup>U. Guler, S. Suslov, A. V. Kildishev, A. Boltasseva, and V. M. Shalaev, *Nanophotonics* **4**, 269 (2015).

<sup>11</sup>S. Kawata, Y. Inouye, and P. Verma, *Nat. Photonics* **3**, 388 (2009).

<sup>12</sup>R. F. Egerton, *Electron Energy-Loss Spectroscopy in the Electron Microscope*, 3rd ed. (Springer Science & Business Media, New York, 2011).

<sup>13</sup>M. N'Gom, J. Ringnalda, J. F. Mansfield, A. Agarwal, N. Kotov, N. J. Zaluzec, and T. B. Norris, *Nano Lett.* **8**, 3200 (2008).

<sup>14</sup>F. G. De Abajo, *Rev. Mod. Phys.* **82**, 209 (2010).

<sup>15</sup>O. Nicoletti, M. Wubs, N. A. Mortensen, W. Sigle, P. A. van Aken, and P. A. Midgley, *Opt. Express* **19**, 15371 (2011).

<sup>16</sup>D. Rossouw, M. Couillard, J. Vickery, E. Kumacheva, and G. A. Botton, *Nano Lett.* **11**, 1499 (2011).

<sup>17</sup>C. Powell and J. Swan, *Phys. Rev.* **115**, 869 (1959).

<sup>18</sup>L. Giannuzzi and F. Stevie, *Micron* **30**, 197 (1999).

<sup>19</sup>R. Erni and N. D. Browning, *Ultramicroscopy* **108**, 84 (2008).

<sup>20</sup>X. Zhou, A. Hörl, A. Trügler, U. Hohenester, T. B. Norris, and A. A. Herzing, *J. Appl. Phys.* **116**, 223101 (2014).

<sup>21</sup>U. Hohenester and A. Trügler, *Comput. Phys. Commun.* **183**, 370 (2012).

<sup>22</sup>See supplementary material at <http://dx.doi.org/10.1063/1.4947442> for the results of ellipsometric analysis and the spatial dependence of the bulk plasmon peak energy.

<sup>23</sup>C. Ahn and O. Krivanek, *EELS Atlas* (Gatan, 1983).

<sup>24</sup>J. Pflüger, J. Fink, W. Weber, K. Bohnen, and G. Crececius, *Phys. Rev. B* **30**, 1155 (1984).

<sup>25</sup>C. Walker, C. Anderson, A. McKinley, N. Brown, and A. Joyce, *Surf. Sci.* **383**, 248 (1997).